SCA-9916

Diffusion Effects on NMR Response of Oil & Water in Rock: Impact of Internal Gradients

John L. Shafer[1], Duncan Mardon[2], and John Gardner[3]
1: Reservoir Management Group, Houston, USA
2: Exxon Exploration Company, Houston, USA
3: Halliburton, Houston, USA

ABSTRACT

Nuclear Magnetic Resonance (NMR) logging in a low permeability gas reservoir has been used to assist standard formation evaluation techniques in identifying productive dry gas zones. Calibration of the NMR log response using core measurements is required for the accurate prediction of permeability and estimates of producible gas and irreducible water saturation. The sandstones that form this reservoir are feldspathic litharenites that are variably cemented with carbonate, chlorite, and quartz. This paper demonstrates the importance of lab NMR measurements at reservoir fluid saturation conditions for core-to-log calibration.

This study contains NMR T_2 measurements on 13 samples at multiple echo spacings at three different fluid saturation states, 100% brine, porous plate desaturated at 50 psi air-brine capillary pressure, and OBM base oil saturated at connate water saturation. The shift in the T_2 distribution with increasing echo spacing allows for the calculation of internal magnetic field gradients. The magnitude of the internal magnetic field gradient is a function of the magnetic susceptibility contrast in the pore space and thus is expected to be saturating fluid, brine or hydrocarbon, dependent. Unexpectedly, we have found that the apparent internal magnetic field gradients for rock samples flushed to connate water saturation with OBM base oil, are as large or larger than the same samples 100% brine saturated.

The magnitude of the calculated internal magnetic field gradients does not appear to correlate with median pore-throat size and has only a weak correlation with the NMR surface relaxivity. Bulk properties such as magnetic susceptibility and iron oxide concentration are not good predictors for the magnitude of the magnetic internal field gradients, which is a pore-based phenomenon. These lab data stress the importance of core-to-log calibration at reservoir fluid saturation.

INTRODUCTION

In the past decade there has been an explosion in the number of talks and journal articles on low field lab NMR measurements of core samples. Most of these papers dealt with rock samples saturated with 100% brine in a homogeneous magnetic field. In recent years more papers have dealt with rock samples saturated with multiple phases as one might find in an oil reservoir, but often these measurements have been in a homogeneous magnetic field. The NMR transverse relaxation, T_2, response of fluids in rock pore space is influenced by magnetic field gradients. A magnetic field gradient can be caused externally by the NMR logging tool, or the NMR lab spectrometer, or internally at the pore scale by mineral-fluid magnetic susceptibility contrasts.

This paper attempts to quantify the magnitude of the apparent internal field gradients with changes in saturating fluids. Stonard (1996) and Zhang (May 1998 & Sept 1998) identified the presence of internal gradients for rocks saturated with both oil and brine but did not quantify the magnitude of the internal gradient. Zhang (Sept. 1998) quantified the magnitude of the internal gradient present in clay slurries with a variety of single-phase fluids. The calculated internal gradient for chlorite slurries ranged from 270 Gauss/cm for brine slurry to 544 Gauss/cm for oil-base-mud (OBM) base oil slurry. Thus, the magnitude of internal magnetic field gradients in rocks was thought to depend on the presence of iron rich clay coating the pores (Zhang, May & Sept 1998; Slot-Petersen, 1998).

The fluids in the pore space in a reservoir environment encountered by NMR logging tools could be connate water, hydrocarbons, and/or drilling mud filtrate. Connate water saturation is achieved by oil displacing brine on a primary drainage capillary pressure path. A simplified model for a water-wet case would be the hydrocarbon in the middle of the pore and surrounded by water. Given that the magnetic susceptibility contrast between oil and water is very small compared to the contrast between brine and rock

surface we would expect the internal field gradients for the oil phase to be very small. In fact, we found that iron rich clay-rich sandstones from the Lower Oligocene Vicksburg trend appear to have as large or larger internal magnetic field gradients when the samples were flushed to connate water saturation with oil-based-mud base oil than the same samples 100% brine saturated.

Understanding the potential magnitude of internal magnetic field gradients is important in core-to-log calibration and for planning NMR logging runs. Knowledge of the relative magnitude of the external gradient caused by NMR logging tool compared to the rock's internal magnetic field gradients is required. Flaum (1996) and Chandler (1994) reported that CMR and MRIL NMR logging tools both have magnetic field gradients of about 20 Gauss/cm. Internal and/or external gradients will affect the NMR response and require careful selection of logging parameters; i.e., position of the gas peak relative to bound vs. free fluid cut-off. Chen (1998) and Akkurt (1998) estimated hydrocarbon viscosity by diffusion from NMR log data. For this approach to work, the rock internal field gradients must be assumed to be insignificant relative to the tool gradient. It would be desirable to be able to use core lithology or mineralogy data to predict where the internal field gradient is, or is not, significant relative to the tool gradient.

Experimental Methods

The measurements reported here are from experiments on cores from two wells (MB and J) in the Vicksburg trend in South Texas. Dodge (1998) and Shafer (1998) have previously reported on lab and log NMR data from other wells in the Vicksburg trend. Both wells were cored with oil-based mud (OBM). The water content in the OBM was maintained at less than 2% with Escaid-110 as the base oil. The core was stored under Escaid and slabbed and plugged with Escaid as the lubricant. Results from the routine core analysis were used to select a sub-set of 10 or 12 preserved plugs from each well for use in the formation evaluation (FE) and reservoir quality program. The FE program consisted of the following core analysis measurements: porosity & permeability at reservoir stress, resistivity (porosity and saturation exponents), single point porous plate capillary pressures (50 psi air-brine), NMR, and mercury injection capillary pressure. To assist in evaluating these core analysis results, material from the ends of the core plugs were used for preparation of thin sections, magnetic susceptibility measurements, and quantitative mineralogy by XRD and XRF (Chakrabarty, 1997). The thin sections were point counted and a SEM was used to identify the type and location of minerals in the pore space. Data from these measurements are summarized in Table 1.

NMR measurements were performed at each saturation state as the core plugs moved through the core analysis protocol; "native-state", 100% brine saturated, desaturated on porous-plate at 50 psi air–brine capillary pressure, and then after resaturation with Escaid (base oil). Since the as-received preserved core plugs were not at 100% saturation due to gas expulsion with core surfacing, the plugs were evacuated and pressure saturated with Escaid. All NMR measurements were obtained with a TE of 0.32ms with the number of echoes and wait times adjusted commensurate with the relaxation time characteristics of each sample. A subset of the 10 or 12 core plugs from each well, were also measured at echo spacings of 1.2ms and 3.6ms to evaluate diffusional effects. T_1 measurements were obtained on two Escaid resaturated core plugs from each well. T_1, T_2, and diffusivity (Do = 6.9 E-06 cm^2/sec) measurements were also obtained on the bulk Escaid.

The NMR measurements were made using a commercially available spectrometer operating at approximately 1 MHz and 25°C. The number of echo trains was adjusted to yield a signal-to-noise ratio of 200. The T_2 measurements were obtained with CPMG pulse sequence and T_1 by inversion recovery. Relaxation time distributions were computed by multi-exponential inversion of the echo data with 51 pre-set decay times logarithmically spaced between 0.1ms and 10,000ms. Multiple inter-echo spacing NMR T_2 measurements on a water sample indicate no significant inhomogeneity in the NMR spectrometer's B_o field.

RESULTS AND DISCUSSION

Rock Properties

The rock properties for the 22 core plugs used in this study are summarized in Table 1. All of these plugs have NMR T_2 measurements at all fluid saturations with echo spacing of 0.32ms, but only 13 of these plugs have the additional two echo-spacings of 1.2 and 3.6ms. Internal gradients were calculated on these

13 samples. At a given core porosity there may be as much as four orders of magnitude in permeability range. The brine saturation obtained by single point porous plate desaturation at 50 psi air-brine capillary pressure is highly correlated with brine permeability, with the data from the two wells falling on the same trend line (Figure 1).

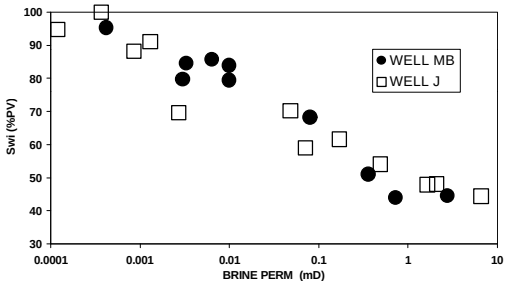

Figure 1. Brine saturation, Swi, at 50 psi air-brine capillary pressure versus brine permeability.

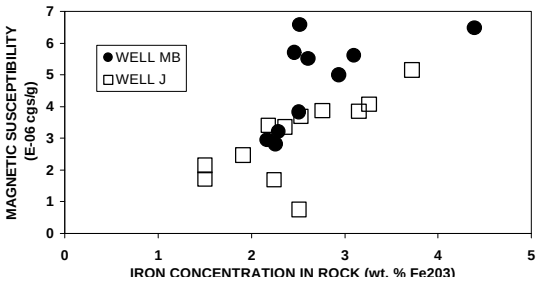

Figure 2. Chemical concentration of iron in core samples reported as wt. % Fe_2O_3 versus the specific magnetic susceptibility.

There appears to be only a weak correlation between the total iron content by chemical analysis of the rock reported as %iron oxide and magnetic susceptibility as illustrated in Figure 2. There is a large variability in magnetic susceptibility for a given iron oxide content. This may be the result of core samples containing different combination of iron containing clays, each with different magnetic susceptibilities. The principal clay minerals based on SEM EDS for Well MB are iron rich chlorite and for Well J iron rich illite-smectite. SEM photomicrographs of the primary clay types in sandstones from each well are shown in Figure 3.

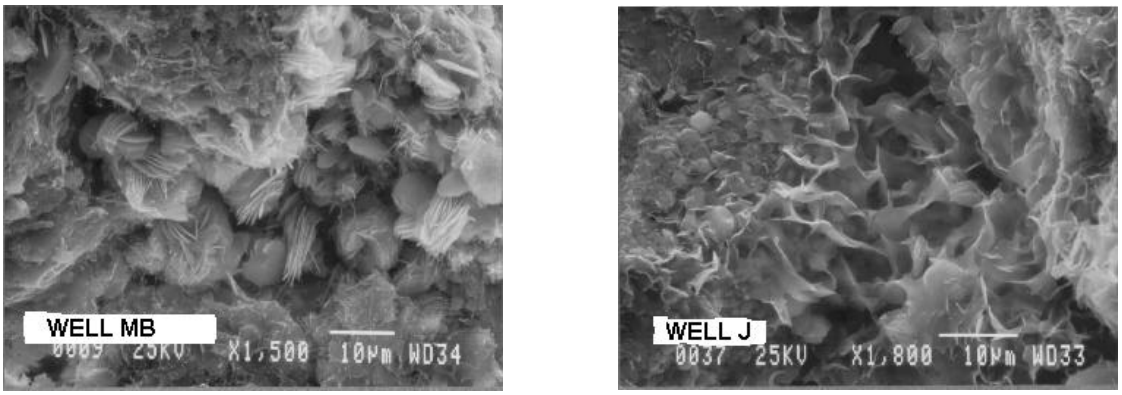

Figure 3. SEM photomicrographs of rock samples show iron rich chlorite grains from Well MB and iron rich illite-smectite grains from Well J.

Relaxation Time Behavior

The measured NMR transverse relaxation rate, $1/T_2$, of fluids in rocks is the sum of three rate terms, bulk fluid relaxation, surface enhanced relaxation, and diffusion-induced dephasing as illustrated in Figure 4. The surface enhanced relaxation rate dominates for the wetting fluid phase, whereas the diffusion term dominates for the fast diffusing molecules such as water and light hydrocarbons. The diffusion-induced dephasing term is a function of the diffusivity of the fluid (D), the inter-echo spacing (TE), magnetic field gradient (G), and the nuclear gyromagnetic ratio (γ). The NMR longitudinal relaxation rate, $1/T_1$, of fluids

in rocks is the sum of only the first two rate terms, bulk fluid relaxation and surface enhanced relaxation. Diffusion-induced dephasing due to magnetic field gradients has no impact on T_1 measurements.

Contributions to Total T_2 Decay Rate for Fluids in Rocks

apparent (measured) relaxation rate	$\frac{1}{T_{2A}} = \frac{1}{T_{2B}} + \frac{1}{T_{2S}} + \frac{1}{T_{2D}}$	
term	**physics**	**dominates***
bulk fluid relaxation (dipole-dipole)	$\frac{1}{T_{2B}} \propto \frac{\text{viscosity}}{\text{temperature}}$	oil
surface-enhanced relaxation	$\frac{1}{T_{2S}} = \rho_2 \left(\frac{S}{V}\right)_{pore}$	water
diffusion-induced dephasing	$\frac{1}{T_{2D}} = \frac{D}{12}(\gamma \cdot G \cdot TE)^2$	both

* assuming water-wet rock

Figure 4. Contributions to total T_2 decay rate for fluids in rocks.

The NMR T_2 distributions, incremental porosity versus T_2 relaxation times, for two samples from each of the two wells, Well MB & Well J, are shown in Figure 5. These plots compare the T_1 and T_2 response for four core plugs at a single saturation state, those of plugs that were initially 100% brine saturated then air desaturated on a porous plate at 50 psi and then resaturated with OBM base oil, Escaid-110, (labeled as "Escaid saturated Swi"). This figure also includes a vertical line representing both the T_2 and the T_1 log mean position of the bulk Escaid peak, since they are similar. These T_2 distributions were obtained at an echo spacing of 0.32ms.

These four sets of relaxation distributions in Figure 5 show that both the long and short relaxation time peaks for the T_2 distributions are shifted about the same degree to shorter relaxation times compared to the T_1 distributions. Since these T_2 distributions were obtained with inter-echo spacing of 0.32ms, the observed shift between T_1 and T_2 may not be due to diffusion-induced dephasing but to the difference in T_1 surface relaxivity, ρ_1, versus T_2 surface relaxivity, ρ_2 (Kleinberg, 1994). The right-most peak in the T_1 distribution that is assumed to represent the Escaid, is at or slightly less than the T_1 position of the bulk Escaid. This would indicate that Escaid appears to be non-wetting, which is consistent with the model of the oil phase surrounded by brine wetted pore surface.

Figure 6 presents the T_2 distributions of the same four plugs at three different saturation states, 100% brine saturated, after desaturation on porous plate at 50 psi air-brine capillary pressure ("Swi"), and resaturated with Escaid-110 (Escaid saturated Swi). The "free-fluid" peak is clearly present at both 100% brine saturated and Escaid resaturated conditions. However, because of surface relaxation, the 100% brine saturated peak is at about a decade shorter T_2 than the Escaid peak.

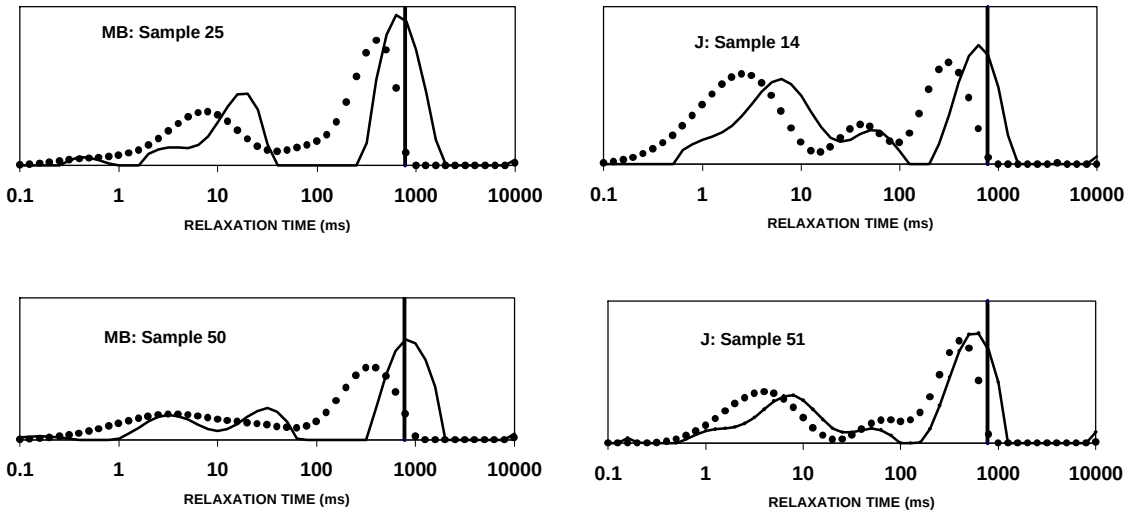

Figure 5. T_1 (solid curve) and T_2 (dotted curve) relaxation time distributions (TE = 0.32 ms) for four samples at the saturation state of Escaid saturated Swi. Vertical line represents position of T_1 & T_2 peak for bulk Escaid.

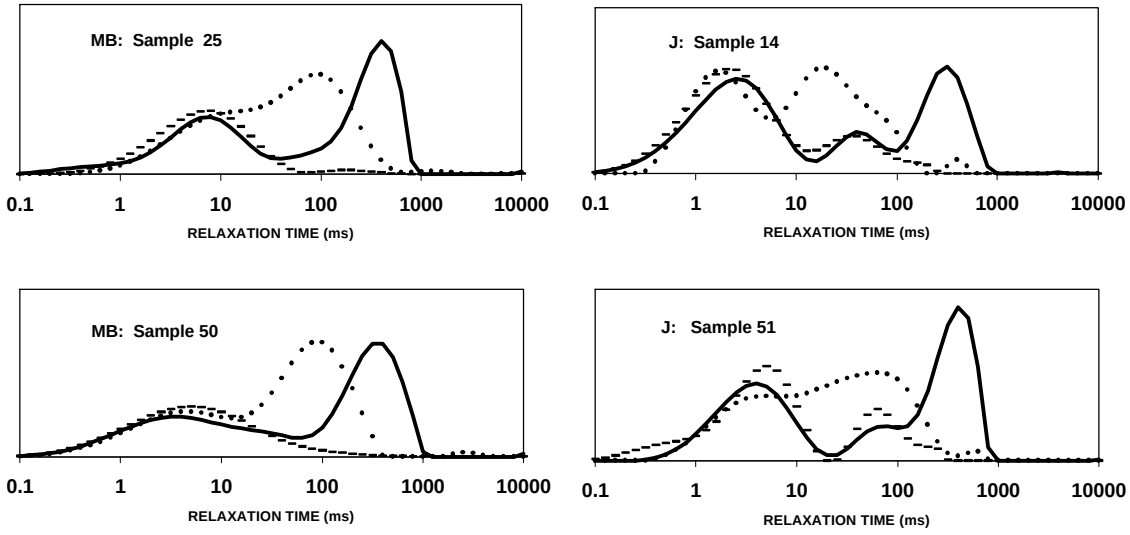

Figure 6. T_2 relaxation time distributions (TE = 0.32ms) for four samples at three saturation states: 100% brine (dotted curve), 50 psi desaturated on porous plate (dashed curve), and Escaid resaturated (solid curve).

Internal Gradients

The internal field gradients, G (Guass/cm), are reported by Hurlimann (1998) and Kleinberg (1996) to be proportional to the magnetic susceptibility contrast, $\Delta\chi$, and the magnetic field strength, B_o, and inversely proportional to distance over which the magnetic field varies (equation 1):

$$G = \Delta\chi * B_o/R \qquad (1)$$

Figure 7 is an illustration of the importance of the diffusion-induced dephasing on the T_2 distribution. Two of the three variables, TE and G, in the diffusion induced rate equation given in Figure 4, are evaluated in Figure 7. The third variable, the fluid self-diffusion coefficient, is set to that for water, 2.3E-05 cm^2/sec. When the magnetic field gradient is 100 Gauss/cm for a short echo spacing of 0.32ms, there is only a minor shift in the T_2 peaks that are greater than 100ms and no detectable shift in the peaks below 33ms, the bound fluid region. With gradient of 100 Gauss/cm, theT_2 peaks in the BVI region are only affected at echo spacings of 1.2ms and greater. However at the longer echo spacings, the fast decay portion of the signal is lost as will be discussed later.

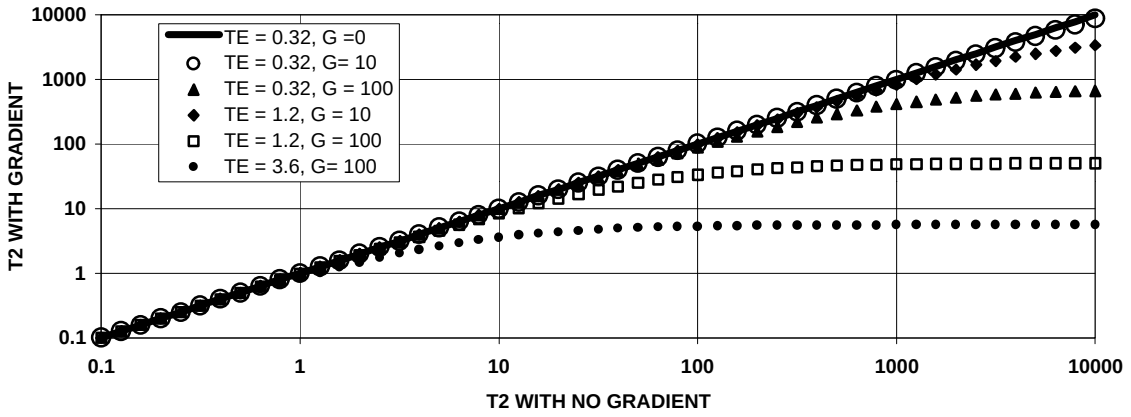

Figure 7. Shift in T_2 peak caused by diffusion effects in a magnetic field gradient.

To quantify the magnitude of the internal gradients, we obtained T_2 measurements at three different echo spacings; 0.32, 1.2, and 3.6ms. The T_2 distributions for the two core plugs from Well MB, #50 and #20, for saturation states of 100% brine and Escaid saturated Swi are presented in Figures 8 & 9. For plug #50, as the inter-echo spacing increases from 0.32ms to 3.6ms the long relaxation portion of the T_2 distribution shifts to shorter relaxation time indicating the presence of internal gradients for both saturation states (Figure 8). However, the shortest relaxation time portion of the T_2 distribution shifts to longer relaxation times (shift to right) as a result of the under sampling of the fast relaxation portion of the decay due to increasing echo spacing; i.e., no data collected before first echo. For plug #20, this shifting of the T_2 distribution to the right with increasing echo spacing is also true for the slow relaxation time peak (Figure 9). Thus low perm rock with a significant fraction of the T_2 distribution below 30 ms will present a data analysis problem: shifting the T_2 distribution to slower relaxation times with increasing echo spacing results in the calculation of a negative internal gradient which has no physical meaning.

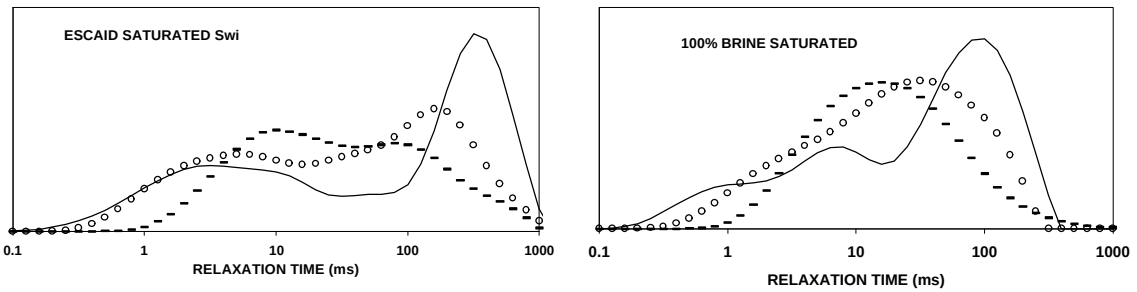

Figure 8. Effect of diffusion in internal gradients for Well MB sample #50 using multiple inter-echo spacings: TE = 0.32 ms (solid curve), TE = 1.2 ms. (circles), TE = 3.6 ms (dashes).

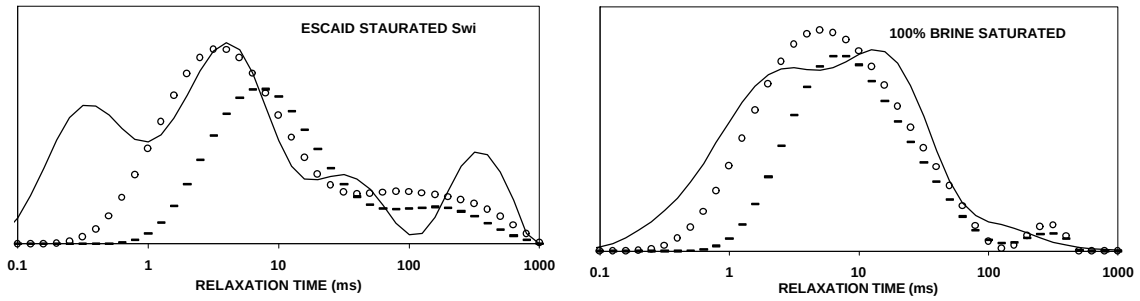

Figure 9. Effect of diffusion in internal gradients for Well MB sample #20 using multiple inter-echo spacings: TE = 0.32 ms (solid curve), TE = 1.2 ms. (circles), TE = 3.6 ms (dashes).

Eight different methods were investigated to quantify the slow relaxing T_2 peak shift with increasing echo spacing. These methods essentially consisted of either defining the "free-fluid" peak position or some form of a mean of the "free-fluid" T_2 distribution. Most of these different methods calculated similar values for the internal gradient but had a large variability in the calculated intrinsic T_2 (intercept on the relaxation rate axis at zero echo spacing and thus no diffusion). We concluded the technique that appeared to be the least subjective in its implementation was to subtract the desaturated echo decay from the 100% brine or the Escaid-saturated Swi echo decays in the time domain for each of the three echo spacings. This difference decay echo train represents the "free-fluid" signal, and was inverted to obtain a T_2 distribution. The geometric mean of the resulting slow relaxation peak was used to determine the shift in T_2 response with increasing echo spacing.

The measured relaxation rate is the sum of three terms, bulk, surface, and diffusion terms, as previously stated (Figure 4). If two NMR T_2 measurements are made under the same experimental conditions except for a change in the inter-echo spacing, TE, (where S = short TE and L = long TE) then the bulk and surface terms cancel when the differential relaxation rate is computed according to equation 2 (Mardon, 1996). The internal gradient, G, after rearranging terms, is proportional to the square root of the slope of relaxation rate vs. TE squared as shown in equation 3.

$$(1/T_{2L} - 1/T_{2S}) = (D/12)(G\gamma)^2 (TE_L^2 - TE_S^2) \quad (2)$$

$$G = ((12/D\gamma^2)*((1/T_{2L} - 1/T_{2S})/(TE_L^2 - TE_S^2)))^{0.5} \quad (3)$$

To determine the apparent internal magnetic field gradient, the T_2 geometric mean of the "free" fluid, brine or Escaid, are converted to a relaxation rate, $1/T_2$, and plotted against the square of the inter-echo time, Figure 10. In the free diffusion region, a straight line is expected. This is not observed here indicating restricted diffusion effects as the inter-echo spacing increases, or as the diffusion distance exceeds the dimension of the pore space (Hurlimann, 1998). Both Zhang (1998) and Appel (1999) have obtained T_2 measurements with a large number of inter-echo spacings and a plot of relaxation rate vs. TE squared becomes non-linear (transition from free to restricted diffusion) when TE typically exceeds about 1ms. Thus, we have used the slope between the first two echo spacings, 0.32 and 1.2 ms, to calculate the internal gradients which should provide a reasonable estimation of G. This is a lower bound estimate since it assumes free diffusion for inter-echo spacings up to 1.2 ms. If the transition to restricted diffusion starts below 1.2ms, then the free diffusion region would have a higher slope and thus a higher calculated gradient. As seen in Figure 10, the slopes between 0.32ms and 1.2 ms are positive for the Escaid saturated Swi samples but not always so for the 100% brine samples. The negative slopes are the result of the under sampling of the fast relaxation portion of the decay due to increasing echo spacing resulting in a shift of the T_2 distribution to slower relaxation times.

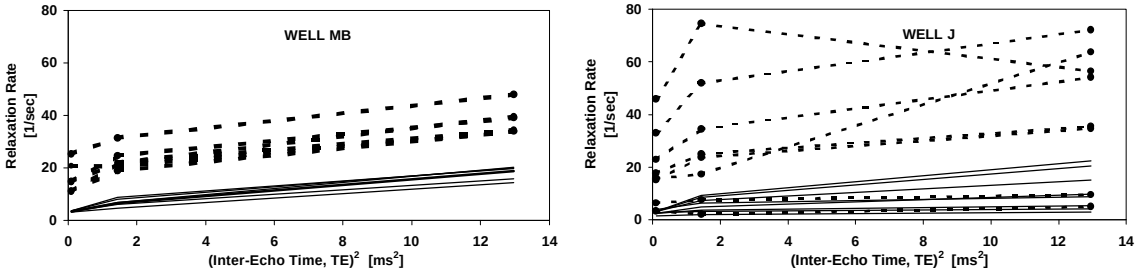

Figure 10. Free fluid diffusion effects for Wells MB and J for Escaid saturated Swi samples (solid lines) and 100% brine samples (dotted lines).

The calculated apparent gradients are provided in Table 1 and plotted in Figure 11 versus the intrinsic T_2 for the samples from both wells. The internal gradient ranged from about 25 to 100 Gauss/cm. If the Escaid in the resaturated Swi samples is not relaxed by the pore surface, then the T_2 intrinsic should equal to the T_2 of the bulk Escaid which is about 800 ms. Most samples display an intrinsic T_2 significantly less than that of bulk Escaid. A cross-plot of the calculated apparent gradients for the 100% brine saturated samples versus the Escaid saturated Swi samples is presented in Figure 12. The calculated apparent gradients for the Escaid saturated Swi samples are generally equal to or greater than the 100% brine saturated samples.

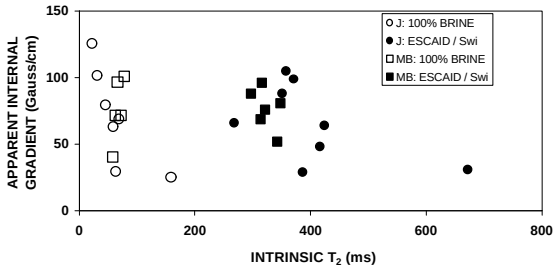

Figure 11 Calculated internal gradients from the slope of the 0.32ms and the 1.2 ms inter-echo spacing data for both wells.

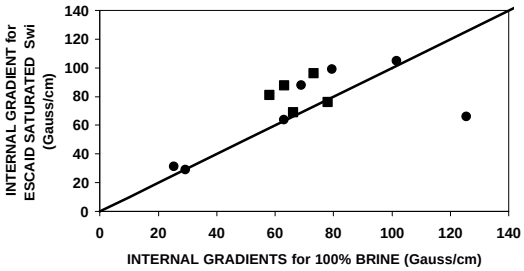

Figure 12. Calculated internal gradients for the "free fluid" in 100% brine saturated samples versus Escaid saturated Swi samples for Well MB (squares) and Well J (circles).

The calculated internal gradients for the Escaid saturated Swi samples from both wells have been compared with the pseudo surface relaxivity, ρ, in Figure 13. The pseudo surface relaxivity was determined by the factor required to rescale the mercury injection capillary pressure data to the NMR T_2 distribution by the method described by Marschall (1995). There is a weak positive correlation between the surface relaxivity and the internal gradient. We had expected that the pore lining iron rich clay minerals that would increase the surface relaxivity (Dodge, 1995) would also cause larger internal magnetic gradients but this was not observed. Surprisingly there is also no apparent correlation between internal gradients and the median pore throat diameter as determined by mercury injection capillary pressure data (Figure 14).

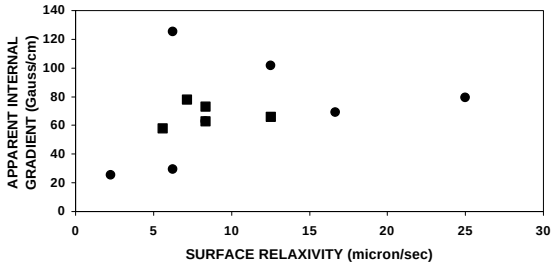

Figure 13. Surface relaxivity, ρ, versus internal magnetic gradient for samples from Well MB (squares) and Well J (circles).

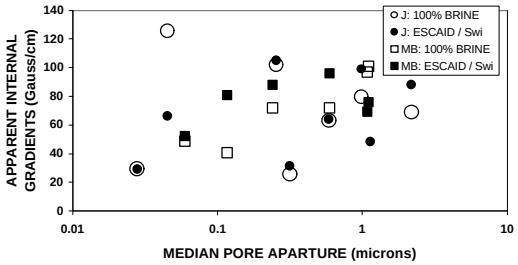

Figure 14. Median pore throat diameter versus internal magnetic gradient for samples from Well MB (squares) and Well J (circles).

The apparent internal gradients as determined from the diffusion effects exhibited by different pore "free-fluid" saturations, do not appear to be consistent with the originally posed simplified model of hydrocarbon in the middle of the pore and surrounded by water. The relative magnitude of the calculated internal gradients for the free fluid, Escaid versus brine, would be indicative of a magnetic susceptibility contrast between fluid and rock surface for both. One explanation may be that when these Vicksburg core plugs were desaturated at a capillary pressure of 50 psi and then resaturated with Escaid, the Escaid is actually in contact with the tips of the clays sticking into the pore space (Zhang, May 1998 & Sept 1998).

CONCLUSIONS

We obtained multi inter-echo spacing NMR T_2 distributions on 13 core plugs from two different wells in the Lower Oligocene Vicksburg Trend at four different saturation states. The main results of this study are as follows:

- It was difficult to unambiguously quantify shifts in the T_2 distribution for the lower permeability samples because of the under sampling of the fast relaxation portion of the decay at larger echo-spacings.
- The calculated apparent internal magnetic field gradients for the region of the pore space occupied by the movable "free-fluid" fraction for the Escaid saturated Swi samples is equal to or greater than the 100% brine saturated samples.
- For these complex mineralogical samples studied, there appears to be little correlation between bulk rock properties (i.e., iron concentration) with magnetic susceptibility, the calculated internal magnetic field gradients, and the surface relaxivity. There is only a weak positive correlation between internal gradient and surface relaxivity.
- Forward modeling of the NMR log response for these Lower Oligocene Vicksburg rocks may be difficult, and it would appear laboratory NMR measurements with reservoir fluid saturation would be required for core-to-log calibration.

ACKNOWLEDGMENTS

We wish to thank and acknowledge the following for their contributions to this paper: Lee Esch of Exxon Production Research for his reservoir quality assessment of these Vicksburg wells, Bill Reese of Exxon Production Research for quantitative mineralogy, and Marcelino Bernardo of Exxon Corporate Research for his measurement of the self-diffusion coefficient of Escaid by PFG NMR. We also thank Exxon and Halliburton for their support and approval to publish this paper.

REFERENCES

Akkurt, R., Mardon, D., Gardner, J. S., Marschall, D. M., and Solanet, F., 1998, Enhanced Diffusion: Expanding the Range of NMR Direct Hydrocarbon-Typing Applications, 39th Annual Symposium of SPWLA, Keystone Resort, CO., May 26-29. Paper GG.

Appel, M., Freeman, J., Perkins, R. B., Hofman, J. P., Looyestijn, W. J., Slijkerman, W. F. J., amd Volokitin, Y., 1999, Restricted diffusion and Internal Magnetic Field Gradients, 40th Annual Symposium of SPWLA, Oslo, Norway, May 30-June 1.

Chakrabarty, T., and Longo, J., 1997, A New Method for Mineral Quantification to Aid in Hydrocarbon Exploration and Exploitation, *Journal of Canadian Petroleum Technology*, December, vol 36, No. 11, pp 15-21.

Chandler, R. N., Drack, E. D., Miller, M. N. , and Prammer, M. G., 1994, Improved Log Quality with a Dual-Frequency Pulsed NMR Tool, SPE 28365, 69th SPE ACTE, New Orleans, September 25-28.

Chen S., Olima, O. Gamin, H., Georgi, D. T., and Minetto, J. C., 1998, Estimation of Hydrocarbon Viscosity with Multiple TE Dual Wait Time MRIL Logs, SPE 49009, SPE ATCE, New Orleans, September 27-30.

Dodge, W. S., Guzman-Garcia, A. G., Noble, D. A., LaVigne, J., and Akkurt, A., 1998, A Case Study Demonstrating How NMR Logging Reduces Completion Uncertainties in Low Porosity Tight Gas Sands Reservoirs, 39th Annual Symposium of SPWLA, Keystone Resort, CO., May 26-29.

Dodge, W. S., Shafer, J. L., and Guzman-Garcia, A. G., and Noble, D. A., 1995, Core and Log NMR Measurements of an Iron-Rich, Glauconitic Sandstone Reservoir, 36th Annual Symposium of SPWLA, Paris, Fr., June 26-29.

Flaum, C., Kleinberg, R.L., and Hurlimann, M. D., 1996, Identification of Gas with the Combinable Magnetic Resonance Tool (CMR), 37th Annual Symposium of SPWLA, New Orleans, LA, June 16-19

Hurlimann, M. D., 1998, Effective Gradients In Porous Media Due To Susceptibility Differences, *Journal of Magnetic Resonance*, 131, 232-240.

Kleinberg, R. L., Kenyon, W. E., and Mitra, P. P., 1994, Mechanism of NMR Relaxation of Fluids in Rock, *Journal of Magnetic Resonance*, 108, 206-214.

Kleinberg, R. L. and Vinegar, H. J., 1996, NMR Properties Of Reservoir Fluids, *The Log Analyst*, Nov.-Dec.

Mardon, D., Gardner, J. S., Coates, G. R., and Vinegar, H. J., 1996, Experimental Study of Diffusion and Relaxation of Oil-Water Mixtures in Model Porous Media, 37th Annual Symposium of SPWLA, New Orleans, LA, June 16-19

Marschall, D., Gardner, J. S., Mardon, D., and Coates, G. R., 1995, Method for Correlating NMR Relaxometry and Mercury Injection Data, 1995, International Symposium of the Society of Core Analysts, San Francisco, CA, September 12-14.

Shafer J. L., Dodge, W. S., and Noble, D. A., 1998, NMR Case Study: Core-to-Log Calibration in a Low Permeability Gas Reservoir, Abu Dhabi SCAL Forum, Abu Dhabi, UAE, October 14-15.

Slot-Petersen, C., Eidesmo, T., Rueslatten, H, and White, J., 1998, NMR Formation Evaluation Applications in a Complex Low-Resistivity Hydrocarbon Reservoir, International Symposium of the Society of Core Analysts, The Hague, The Netherlands, September 14-16, paper SCA-9821.

Stonard, S. W., LaTorraca, G. A., and Dunn, K. J., 1996, Effects of Magnetic Susceptibility Contrasts on Oil and Water Saturation Determinations By NMR T_2 Laboratory and Well Log Measurements, 1996, International Symposium of the Society of Core Analysts, San Francisco, CA, September 12-14.

Zhang, G. Q., Hirasaki, G. J., and House, W. V., 1998, Diffusion in Internal Field Gradients, International Symposium of the Society of Core Analysts, The Hague, The Netherlands, September 14-16.

Zhang, G. Q., Lo, S.-W., Huang, C.C., Hirasaki, G.J., Kobayashi, R., and House, W.V., 1998, Some Exceptions to Default NMR Rock and Fluid Properties, 39th Annual Symposium of SPWLA, May 26-29, 1998, Keystone Resort, CO.

TABLE 1 VICKSBURG ROCK PROPERTIES

					POROUS	MICP				Clay Mineralogy					NMR INTERNAL GRADIENTS			
				Resistivity	PLATE		median	Magnetic					NMR	100%brine		Escaid / Swi	
Plug	Lithology	Plug Porosity	Kb	Porosity	Swi/a-b Pc	Swi/a-b Pc	pore dia.	suscept	%Fe2O3	Chlorite	Illite & Smectite	total clay	Surface Relaxivity	Gradient	T2 Intrinsic	Gradient	T2 Intrinsic
#		(%BV)	(mD)	Exponent	50psi (%PV)	50psi (%PV)	aperture (microns)	(cgs/g) *E-06	(wt. %)	(wt. %)	(wt. %)	(wt. %)	(micron/s)	(G/cm)	(msec)	(G/cm)	(msec)
WELL MB																	
14	QPAA	11.7	0.003	2.13	84.6	90	0.06	5.7	2.5	6	7	14	2.5	negative	48	52	342
20	QPAA	14.2	0.006	2.07	85.7	86	0.12	5.5	2.6	6	8	15	6.3	58	41	81	348
25	QPAA	18.1	2.75	2.06	44.6	43	1.08	2.9	2.2	5	6	11	10.0	66	97	69	314
28	QPAA	11.2	0.01	2.17	79.4	74	0.24	3.8	2.5	6	6	12	5.0	63	72	88	297
32	QPAA	15.9	0.36	2.13	51	52	0.59	3.2	2.3	6	7	13	6.3	73	72	96	315
50	QPAA	14.5	0.73	2.15	44	44	1.10	2.8	2.3	5	6	11	6.3	78	101	76	321
22	QPAA	11.2	0.003	2.11	79.7	88	0.14	6.6	2.5	6	3	11	4.0	N.A.	N.A.	N.A.	N.A.
37	FW	14.9	<0.001	2.21	95.2	100	0.03	6.5	4.4	8	24	32	10.0	N.A.	N.A.	N.A.	N.A.
44	QPAA	16	0.01	2.11	83.9	85	0.17	5.6	3.1	8	11	19	5.0	N.A.	N.A.	N.A.	N.A.
48	QPAA	16.8	0.08	2.17	68.3	63	0.31	5.0	2.9	7	8	15	6.3	N.A.	N.A.	N.A.	N.A.
WELL J																	
14	QRAA	25	0.048	2.32	70.2	62	0.26	3.9	3.2	6	11	23	10.0	60	321	105	357
24	QRAA	9.1	0.003	2.36	69.7	62	0.32	0.8	2.5	1	2	5	2.0	16	658	31	671
31	QRAA	17.4	1.64	2.04	47.9	44	1.14	1.7	2.2	3	4	9	10.0	23	404	48	416
46	QRAA	21.2	6.57	1.97	44.5	38	2.19	2.5	1.9	5	TR	8	15.8	48	325	88	351
50	QRAA	20.2	<0.001	2.16	94.8	93	0.05	5.2	3.7	7	18	31	6.3	31	258	66	268
51	FW	18.2	0.071	2.21	59.1	51	0.59	2.2	1.5	4	1	8	6.3	37	404	64	424
55	FW	18.9	<0.001	2.07	100	100	0.03	4.1	3.3	4	27	37	6.3	16	383	29	386
61	QRAA	23.7	0.49	2.19	54.1	46	0.99	3.4	2.4	5	5	14	15.8	57	337	99	371
8	QRAA	24.6	0.17	2.09	61.6	55	0.43	3.9	2.8	6	7	17	15.8	N.A.	N.A.	N.A.	N.A.
9	QRAA	24.9	2.08	2	48.1	42	1.45	3.4	2.2	5	3	11	19.9	N.A.	N.A.	N.A.	N.A.
19	QRAA	22.1	0.001	2.29	91.1	91	0.09	3.7	2.5	5	11	22	6.3	N.A.	N.A.	N.A.	N.A.
34	QRAA	9.1	0.001	2.07	88.2	97	0.14	1.7	1.5	1	4	6	4.0	N.A.	N.A.	N.A.	N.A.

NOTES: Lithology Key: QPAA = quartz-poor arkosic arenites, QRAA quartz-rich arkosic arenites, FW = feldspathic wackes